The Effect of Fe, Mn and Trace Elements on Precipitation in Al-Mg-Si Alloy

Zeqin Liang[1], Cynthia Sing Ting Chang[1], Nelia Wanderka[1], John Banhart[1] and Juergen Hirsch[2]

[1] Institute of Applied Material, Helmholtz Center Berlin for Material and Energy, Hahn-Meitner-Platz 1, Germany

[2] Hydro Aluminium Deutschland GmbH, Georg-von-Boeselager Straße 21, Germany

The effect of Fe, Mn and other trace elements on the ageing response of Al-Mg-Si alloy has been investigated. Three alloys were used: Al-0.4wt%-1.0wt%Si alloy with a very low level of impurities, Al-0.4wt%-1.0wt%Si with 0.25wt%Fe and 0.08%Mn and a 6016 commercial alloy containing further elements. Samples were solution heat treated and then quenched in different media. After quenching, samples were artificially aged. Their ageing responses were studied by using microhardness. Differential Scanning Calorimetry (DSC) was performed in order to investigate their precipitation behavior. Moreover, the morphology of the precipitates and intermetallic compounds were characterised by using Transmission Electron Microscopy (TEM) and Scanning Electron Microscopy (SEM). Result shows that, at the paint bake condition, the 6016 alloy has the largest number density of β'', and this correlates to the fact that 6016 alloy has the fastest ageing response, while the alloy containing Fe and Mn has the slowest. DSC shows that the precipitation behavior after solid solution treatment for 6016 and the alloy containing Fe and Mn is not sensitive to the cooling rates. The presence of Fe and Mn lowers the Si content in the matrix, which is necessary for the formation of β'' during ageing. On the other hand, the presence of the trace elements promotes the formation of β'' and increases the hardening rate during ageing despite the fact of the presence of the intermetallic compounds.

Keywords: Al-Mg-Si alloys; Fe Mn and trace elements; intermetallic phases; age hardening; precipitation

1. Introduction

Al-Mg-Si alloys are now increasingly being used in automotive industry, e.g. for car body panels. When used in this way, paint baking and precipitation hardening are carried out simultaneously. This process can be optimised by tuning both the composition of the alloy and the heat treatments. It has been reported that the strength after paint baking is affected by small changes of the Mg and Si content, Mg/Si ratio and the presence of additional elements [1–4]. On the other hand, an appropriate heat treatment is required to reduce the negative strength response caused by natural pre-ageing, i.e. 'room storage' before ageing [5,6]. These two variables are inter-linked with each other. In order to reduce testing time and cost, a model that can simulate a through-process starting from casting to rolling, stamping and paint baking is necessary. However, such modeling is complicated on the one hand by the transformations occurring during natural ageing and their effect on subsequent trace element precipitation. Up to now, this is not fully understood [7]. The other hand, the effects of other elements on precipitation have to be known, which is why in this work the influence of Fe, Mn and other trace elements on the precipitation of Al-Mg-Si alloys during paint bake has been investigated.

2. Experimental

Two experimental aluminum alloys and the commercial alloy 6016 were investigated, both provided by Hydro Aluminum Bonn. The compositions tested by OEM are listed in table 1. For the experimental alloys, the as-received materials were extruded to 1 mm thickness, while the commercial 6016 alloy was hot and cold rolled to 1 mm thickness after casting and homogenization.

The samples were first solutionised in an argon atmosphere at 540°C for 1 hour and then quenched using different media, namely ice water, water 20°C and air to vary the quenching rate.

The samples that were quenched in ice water either underwent natural ageing at 20°C or were artificially aged at 180ºC in an oil bath. Microhardness was measured in various stages of ageing. Since a rapid increase of hardness is expected for natural ageing times shorter than 1000 min, real time measurements were performed for short times. After 1000 min of natural ageing, an average hardness value was obtained from 10 measurements in larger intervals. Differential scanning calorimetry (DSC) was performed in a NETZSCH STA 404A. The DSC samples were cut and ground to identical discs (scatter in weight: ±2%) before solutionising. After quenching in different media, samples were inserted into the DSC and the run was started within 3 min. Aluminum samples of 99.99% purity and the same mass were measured to obtain data for the baseline correction for each alloy sample. Characterization of the size and number density of the precipitates was done by transmission electron microscopy (TEM) using a Philips EM400. Samples in the paint baked condition, i.e. artificially aged for 20 min after ice-water quenching, were mechanically polished down to about 80 μm and then thinned by twin-jet electro-polishing technique in a Tenupol cell with a solution of 30% nitric acid and 70% methanol at −30ºC applying a voltage of 15V. The composition of the intermetallic phases was measured by energy dispersive X-ray analysis (EDX) in a scanning electron microscope.

Table 1 compositions of the experimental alloys

Alloy	Compositions (wt%)								
	Mg	Si	Fe	Mn	Cu	Cr	Zn	Ti	Al
Alloy E	0.4	1.0							Balance
Alloy 4	0.4	1.0	0.25	0.08					Balance
Alloy 5 (6016)	0.4	1.0	0.28	0.07	0.0412	0.0113	0.0106	0.0192	Balance

3. Results

3.1 hardening behaviour

Fig. 1(a) shows the hardening course during natural ageing of the three alloys. Alloy 5 has the highest initial hardness value, while alloy 4 shows the lowest. All 3 alloys show a similar trend with 3 segments in which there is a near-linear relationship between hardness and the logarithm of time (stage 1: from about 10 min to 1000 min; stage 2: from 1000 min to 20000 min; stage 3: after 20000 min).

(a)   (b)
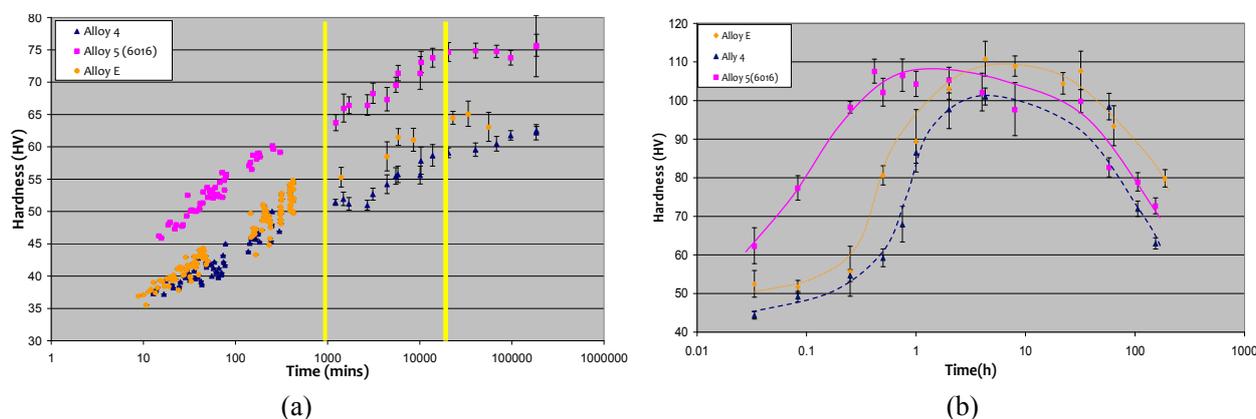
Fig. 1. Hardness evolution during (a) natural ageing (b) immediate artificial ageing of the three alloys after solutionising and quenching in ice water.

Fig. 1 (b) shows the hardening evolution during artificial ageing. Alloy 5 has the fastest artificial ageing response and reaches its peak hardness after 30 min. In contrast, alloys 4 and E take about 8 hours to reach their peak-aged condition. It is also found that alloys 5 and E have similar peak hardnesses of ~110 HV, while for alloy 4 the peak hardness is 102 HV only. For alloys E and 4, the

increase of hardness is slow in the first 15min of artificial ageing, after which the hardening process accelerates. This initially slow age hardening stage is not observed in alloy 5.

3.2 Identification of the intermetallic phases

Since no intermetallic phases were found in alloy E, only alloys 4 and 5 in the as-received condition were investigated in the SEM. Different sizes and distributions of intermetallic phases were found as shown in Fig. 2. By EDX analysis the compositions of these intermetallic phases were obtained. They are grouped according to their composition in Table 2. Both alloys contain Si-rich phases. In alloy 4 the size of the Si-rich phase is smaller than in alloy 5.

| | (a) | | | (b) | |
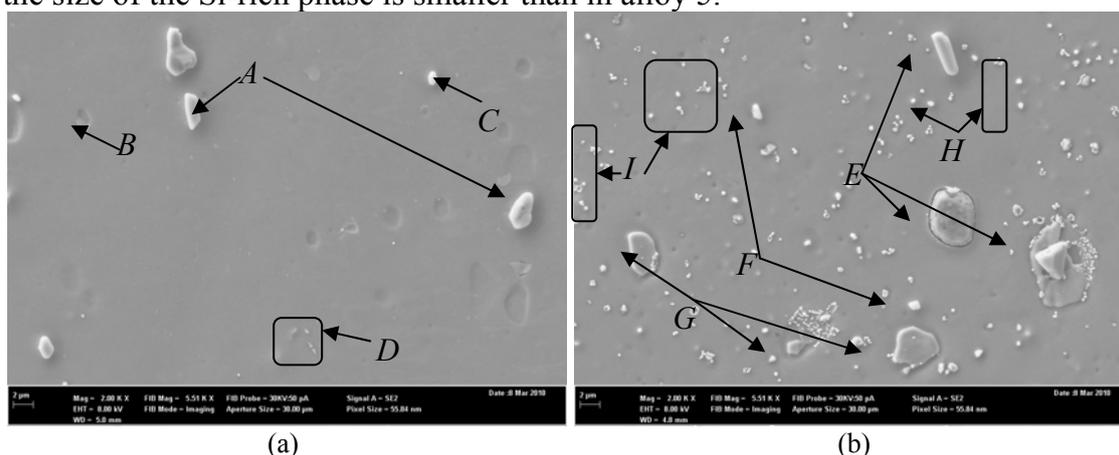
Fig. 2. SEM images of (a) alloy 4 and (b) alloy 5 showing intermetallic phases

Table 2. Intermetallic phases as analysed by SEM and EDX analysis.

	main elements (in the order of abundance)	size range (μm)	Si (at.%)	Mg (at.%)	marker in Fig. 2
4	Si	2-6	75		A
	Al-Si-Fe-Mn	1	7		B
	Al-Si	1-2	40		C
	Al-Si-Mg	0.2-0.4	5	1	D
5	Si	2-10	75		E
	Si-Mg	2-3	68	32	F
	Al-Si-Mg-Fe-Mn	1-2	23	13	G
	Al-Si	0.2-0.5	45		H
	Al-Si-Mg-Cu	0.5-1	3	0.6	I

3.3 Characterization of the metastable phases

(a)   (b)   (c)
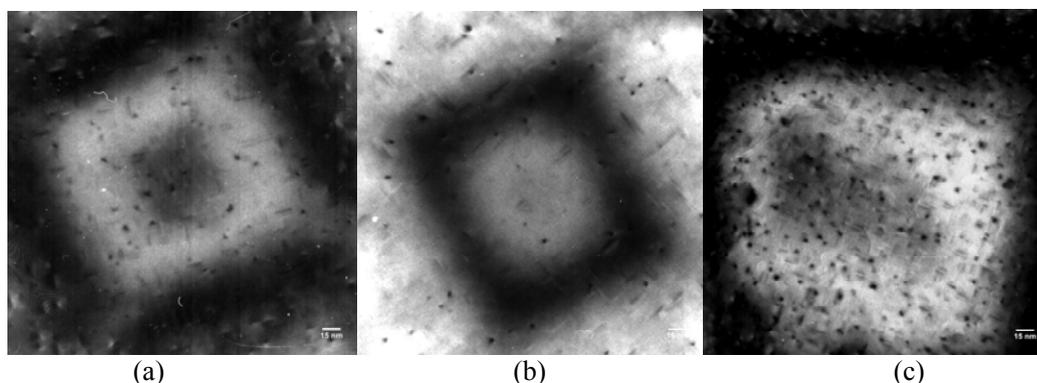
Fig. 3. TEM bright field images and of samples in the paint baked condition (1hr SHT@540 + 20min AA@180 °C). (a) alloy E (b) alloy 4 (c) alloy 5(6016).

Fig. 3 shows bright field TEM images of samples that were solutionised at 540°C for 1 hour, then ice-water quenched and artificially aged at 180°C for 20 min. The average size and number density of the precipitates in all the alloys are summarised in Table 3. It is found that alloy 5 has the highest

number density but smallest average length of precipitates, while alloy 4 shows the lowest number density but largest average length of precipitates.

Table 3. Average length and number density of samples in paint baked condition

alloy code	number density ($\times 10^{20}$m^{-3})	average length (nm)
E	5.4	6.4 ± 0.8
4	2.2	11.3 ± 3.2
5	10.6	3.3 ± 0.5

3.4 Thermal analysis of precipitation

After quenching in different media (ice water, water at 20°C and air), the samples were put into the DSC and heated at a constant heating rate of 10 K/min as shown in Fig. 4. The main peaks and troughs that represent the formation and dissolution of phases during the DSC run are marked in Fig. 4 by A: formation of clusters, B: formation of GP zones, C dissolution of previously formed precipitates, D: formation of β'', E: formation of β' and F: formation of β.

Fig. 4 (a) shows that in alloy E the formation peak of β'' is shifted to higher temperatures with slower cooling rate. Moreover, in air-cooled samples the formation of β' is much more pronounced compared to the samples quenched in ice water or water at 'room temperature'. On the other hand, compared to the results obtained for all three alloys, it can be seen that the quenching rate does not affect the precipitation kinetics so much in alloys 4 and 5 as is does in alloy E, see Figs. 4 (b,c).
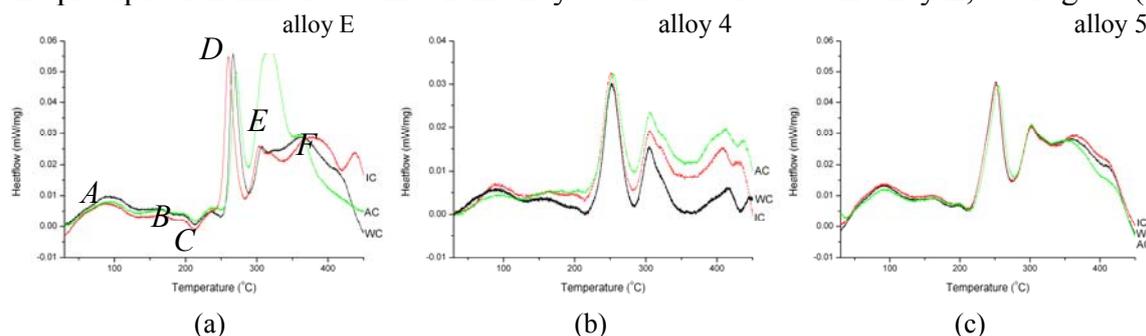
Fig. 4. DSC traces measured at 10 K/min heating rate after quenching in different media of
(a) alloy E, (b) alloy 4, (c) alloy 5.

Apart from the different dependence on cooling rates, the peak position and the heat effect of the β'' peak is also different in alloys E, 4 and 5. The results for ice-water quenched samples are summarised in Table 4. It is found that the onset of β'' formation in alloy E is ~252 °C, which is around 25 K higher than for alloys 4 and 5. Moreover, width of the β'' peak in alloy E is narrower than in alloys 4 and 5.

Table 4. Parameters related to the formation of β" in the different alloys (ice-water quenching applied).

alloy code	onset temperature T_s (°C)	peak temperature T_p (°C)	enthalpy (J/g)
E	252	267	4.93
4	219	252	4.81
5	219	251	6.9

4. Discussion

The effect of Fe, Mn and the trace elements present in Al-Mg-Si alloys can affect precipitation during artificial ageing in two ways: (1) by reducing the level of supersaturation of Mg and Si after solutionising because of the formation of intermetallic compounds, (2) by affecting the diffusion kinetics during artificial ageing. The three alloys show a similar hardening course during natural ageing. It is expected that during natural ageing only clusters form and that these cause the hardening effect. Two kinds of clusters with overlapping formation peaks are shown in Fig. 4 in the area

marked with 'A', in agreement with Refs. 7–9. It has been argued that the first reaction refers to Si clustering, while the second one is regarded as a transformation of the cluster formed earlier, the kinetics of which is dominated by the diffusion of Mg [8]. It is known that the enthalpy of clustering reflects the volume fraction of clusters which form. In Fig. 4 it can be seen that the peak of the clustering reaction in alloy 5 is the largest among the three alloys and therefore it can conclude that alloy 5 forms more clusters than alloys 4 and E during natural ageing. This can also explain the most pronounce hardening effect in alloy 5 during natural ageing, as shown in Fig. 1. During natural ageing, four stages of clustering are observed [7], among which the third stage is a co-clustering stage of Mg and Si and the fourth might be an ordering process. Compared with the different slopes and time scales defined in Fig. 1(a), the hardness evolution associated to the first two linear slopes in these alloys corresponds to stages 3 and 4, applying the numbering given Ref. 7. As there is a delay caused by grinding and polishing of the samples before hardness measurement, stages 1 and 2 of Ref. 7 are not discernable in the hardness course in Fig. 1. Although intermetallic phases containing Mg and Si are present in alloy 5, which will lower the solute content in the matrix, it appears that the presence of trace elements promotes the clustering reaction in alloy 5.

During artificial ageing, alloy 5 shows the fastest hardening response, while alloy 4 shows the slowest. This indicates the possibility that the presence of Fe and Mn in alloy 4 reduces the precipitation rate, while other trace elements accelerate it. In order to understand the effect of Fe, Mn and the other trace elements on precipitation kinetics, a Kissinger-type analysis was applied in which the activation energy is determined from:

$$\ln \frac{T_y^2}{\phi} = \frac{E}{RT_y} + \ln \frac{E}{Rk_0} + \ln \beta_y, \tag{1}$$

where T_y is the temperature at which a given fraction of phase has transformed, ϕ the heating rate during the DSC run, E the activation energy, k_0 the exponential factor, and β_y is close to 1 in the isochronal thermal model [11].
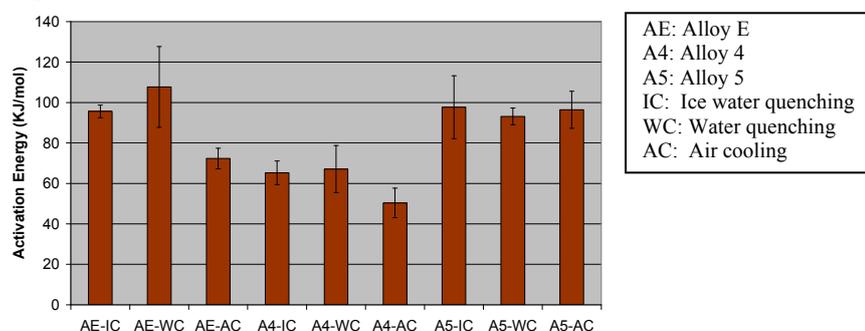
Fig. 5. Activation energy of β'' formation (IC= ice-water cooling ,WC= 'room temperature' water cooling, AC=air cooling).

By using the peak temperature measured at different heating rates (10 K/min, 15 K/min 20 K/min and 30 K/min), the activation energy of the formation of β'' for the three different alloys quenched in different cooling media is calculated. The results are summarised in Fig. 5. The activation energy of the formation of β'' for all the alloys and conditions ranges from ~60 to 105 kJ/mol, which is smaller than the activation energy of Si and Mg diffusion in aluminum i.e., 124kJ/mol and 131kJ/mol, respectively [12]. This agrees with the results obtained in the literature [13,14]. Taking ice-water quenched samples as an example, the activation energy of alloy 4 is the lowest while alloys E and 5 are similar. The explanation for this has to be related to the difference in the impurity content of the alloys. Alloys with lower Si content have found to yield a lower activation energy [15]. It is possible that the presence of intermetallic phases, which lowers the supersaturation of Si in the Al matrix causes a lower value of the activation energy of β''. However, alloy 5 also contains intermetallics

which trap Si from the matrix. The higher value of activation energy that is obtained has to be explained by the presence of trace elements. Up to now, this cannot be fully explained.

As it can be observed from the TEM images, the three alloys possess different number densities and sizes of the precipitates in the paint-baked condition. It can be expected that both the difference in the content of Mg and Si and the presence of other elements will alter the rates of the nucleation and growth of β'' in these three alloys.

Similar to other iso-conversional methods for the calculation of activation energies (such as the Ozawa and Takhour formula), the Kissinger method implies that the reaction can be described as a single process or several process with unique activation energies, so that this method cannot be applied to systems in which the transformation is more complex. As in our work, the nucleation and growth of β'' will be affected by several factors, e.g. solute content and trace elements, etc. A method which takes into account nucleation and growth as separate processes is required. Therefore, in order to obtain a better understanding of the different precipitation kinetics of these three alloys, models involved nucleation and growth should be applied in the future. One method could be as the model by Mittemeijer et al. [16].

5. Conclusions

Both natural and artificial ageing of some model Al-Mg-Si alloys with different impurity levels has been studied.

1. Slower hardening was found in the Al-Mg-Si alloy containing Fe and Mn only, whereas other additional trace elements accelerated hardening.
2. Different precipitate sizes and number densities were found in the three alloys studied in the paint baked condition. This shows that by adding other elements, the nucleation and growth process of the precipitates in the Al-Mg-Si alloy could be further modified.

References

[1] M. Takeda, F. Ohkubo, T.Shirai, K. Fukui: J. Mater. Sci. 33 (1998) 2385-2390.
[2] S. Esmaeili, D.J. Lloyd: Scripta Mater. 50 (2004) 155-158.
[3] A. K. Gupta, D.J. Lloyd, S.A. Court: Mater. Sci. Eng. A316 (2001) 11-17.
[4] J. RØsyet, T.Stene, J.A. Sæter and O. Reiso: Mater. Sci. Forum 519-521 (2006) 239-244.
[5] L. Zhen, S.B. Kang: Mater. Lett. 37 (1998) 349-353.
[6] M. Saga, Y. Sasaki, M. Kikuchi, Z.Yan and M. Matsuo: Mater. Sci. Forum. Vol.217-222(1996) pp. 821-826
[7] J. Banhart, C.S.T. Chang, Z. Liang, N. Wanderka, M.D.H. Lay, A.J. Hill: Adv. Eng. Mater. (2010) in print.
[8] C.S.T Chang and J. Banhart: Met. Mater. Trans A. submitted.
[9] A.K. Gupta and D.J. Lloyd: Met. Mater. Trans A vol. 30A, 3, pp. 879-884 1999.
[10] A. Serizawa, S. Hirosawa and T. Sato: Met. Mater. Trans A vol 39A, 2, pp243-250 2008.
[11] E.J.Mittemeijer: J. Mater. Sci. 27 (1992) 3977-3987.
[12] Kinzoku: Data Book: Japan Inst. Metals, Sendai, Japan, pp.20.
[13] Long Chau Doan, Y. Ohmori and K. Nakai: Mater. Trans JIM, 41 (2000) 300-305.
[14] A.Gaber, M.A. Gaffar, M.S. Mostafa, E.F. Abo Zeid: J. Alloys and Compounds Vol.429 (2007) pp 167-175.
[15] N. Afify, A.Gaber, M.S. Mostafa, Gh. Abbady: J. Alloys and Comp. 462 (2008) 80-87.
[16] F. Liu, F. Sommer, E. J. Mittemeijer: J. Mater. Sci. 39 (2004) 1621-163.